METHODS FOR THE LOCALIZATION OF RADIO SOURCES: APPLICATION TO THE SMOOTH NEPTUNIAN KILOMETRIC RADIATION

H.P. Ladreiter*, Y. Leblanc†, G. K. F. Rabl*, and H. O. Rucker*

Abstract

During the Neptune flyby the Planetary Radio Astronomy (PRA) experiment aboard Voyager 2 detected smooth and bursty radio emissions. Both recur in a rather regular pattern with a 16.1 hour period (the Neptunian spin period). The existence of both, right–hand (RH) and left–hand (LH) polarized smooth emissions is consistent with two sources (one in each hemisphere) which radiate independently in the R–X mode.

The specific geometrical conditions during the Voyager 2 Neptune encounter are used to locate the Neptunian radio sources (the OTD2 magnetic field model is assumed) . **(a)** We have taken advantage of the close encounter distance of Voyager 2 over the northern pole of Neptune to locate the northern hemispheric radio source via visibility studies. We calculated the radio horizon for different spacecraft positions near the encounter. This allowed us to derive source positions without any assumption on the emission beaming. **(b)** We have assumed a straight line propagation and an emission beamed into hollow cones to determine the source location and beaming properties of the northern source. **(c)** The southern hemispheric sources have been derived based on a method using the large spacecraft excursions in the southern magnetic hemisphere.

All the results lead us to conclude that the southern and northern sources are located at conjugate foot points at high magnetic latitudes in a limited range of longitudes. The emission's beaming is described in terms of hollow cones with large half opening angles.

1 Introduction

In August 1989, Neptune was discovered by the planetary radio astronomy (PRA) experiment [Warwick et al., 1977] to be the fifth radio–emitting planet in our solar system. Like the other radio emitters (Earth, Jupiter, Saturn, and Uranus), Neptune exhibits

*Space Research Institute of the Austrian Academy of Sciences, A–8010 Graz, Austria
†Observatoire de Paris, F–92195 Meudon, France and University of Colorado, Boulder, USA

a complex radio spectrum. Several independently radiating radio components were detected: A bursty component was the first radio signal detected from Neptune; it shows the planetary spin period of about 16 hours. The bursts are very short (a few seconds) and occur from 600 kHz to about 1300 kHz [Warwick et al., 1989]. The smoothly varying emission consists of at least three components: One component was observed only a few rotations around closest approach (August 25, 1989) and lies in the frequency range from about 600 kHz to 800 kHz; a second component was observed at times of magnetic equator crossings and occurs from a few tens of hertz to about 56 kHz. It is referred to as nonthermal continuum radiation [Kurth et al., 1990]. The main emission, however, occurs in a larger frequency range from 20 kHz to about 900 kHz (at times near encounter) and was clearly observed 10 days around the encounter. This component of the Neptunian kilometric radiation (hereafter NKR) will be analyzed in detail in this paper.

We will briefly discuss in section 2 the phenomenology of the smooth emission, in particular the state of polarization and the occurrence of the radiation in terms of planetocentric coordinates. In section 3 we introduce the offset tilted dipole (OTD2 model, N.F. Ness, private communication) and discuss its relevance to the source location of the emission. In section 4 we infer the different methods to derive the locations of the radio–emitting regions within the magnetosphere of Neptune. Section 5 ends up with a discussion.

2 Morphology of smooth NKR

The radio observations were made by the planetary radio astronomy (PRA) experiment [Warwick et al., 1977]. This experiment consists of two monopole antennas that measure the intensity and polarization of the radio signal. Every 6 s, the PRA receiver scans 198 fixed frequency channels from 1.2 kHz up to about 40 MHz. During the observations of Neptune only the low–frequency band receiver was operating, from 1.2 kHz to 1326 kHz.

2.1 The smooth recurrent NKR pattern

The Neptunian radio emissions, like those of the other radio planets, are repetitive with the planet's spin period. This is a consequence of the tilt of the magnetic dipole with respect to the rotational axis and of the locations of the radio sources. The regular modulation of the emission has been used to determine accurately the rotation period of the planet, which was found to be 16.105 ± 0.006 hours [Lecacheux et al., 1992, submitted to *Journal of Geophysical Research*]. The smooth NKR pattern is also repetitive and shows no significant local time effect (when comparing Voyager 2 (V2) inbound and outbound observations). Figure 1a shows a typical PRA dynamic spectrum of the smooth emission as observed during one Neptunian rotation (on day of year (DOY) 236), shortly before the closest approach. The emission activity extends from about 320° to 160° NLS (Neptune longitude system), lasting more than 8 hours during each rotation. The emission occurred in a frequency range from 20 kHz to about 600 kHz.

The polarization of the smooth emission is complex. The sense of circular polarization has been determined by taking into account the tilt of the electric plane of the antenna with

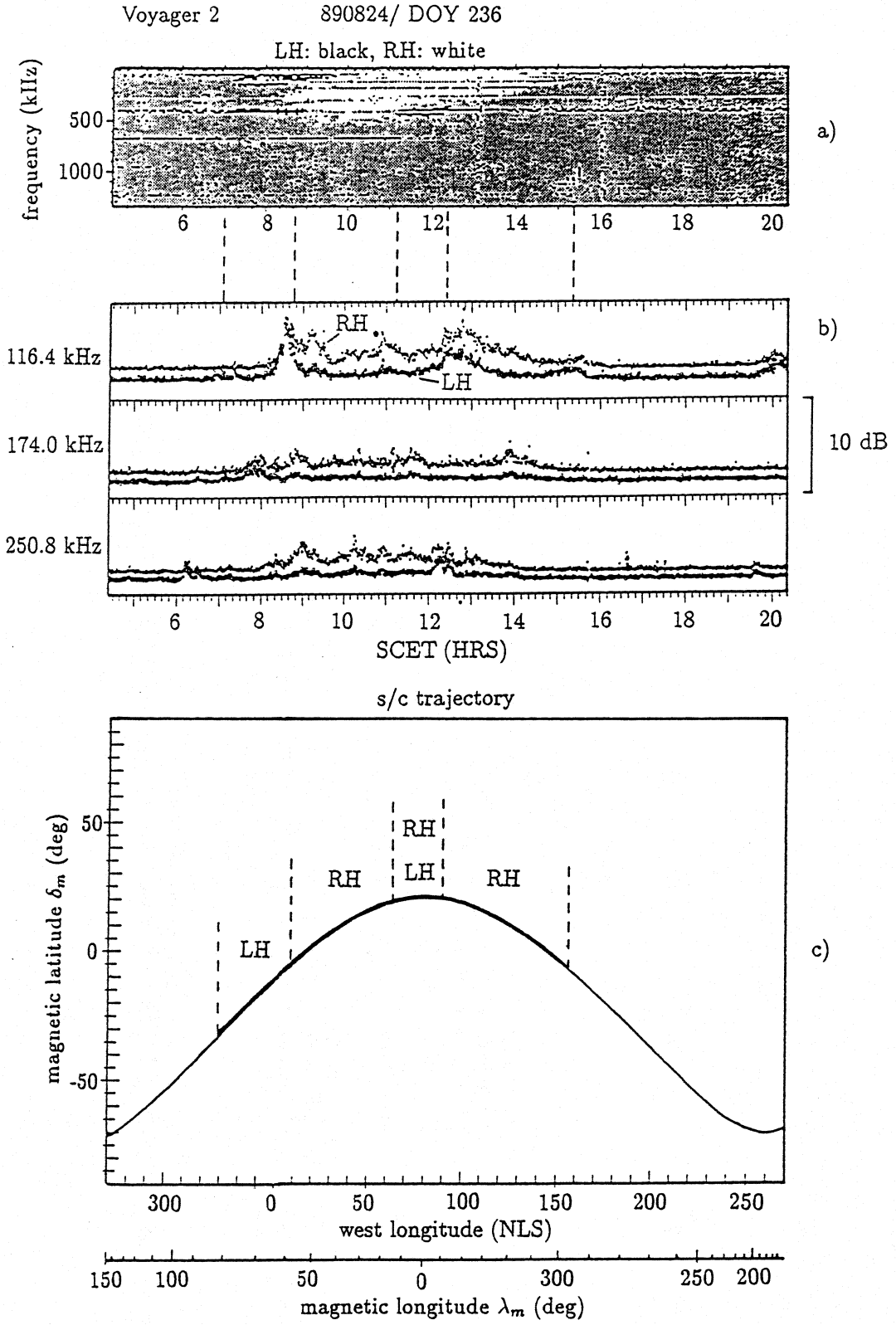

Figure 1: The smooth Neptunian kilometric radiation during one rotation: (a) dynamic spectrum, (b) intensity versus time at three fixed frequencies, and (c) spacecraft magnetic latitude. The episodes of LH and RH emission are indicated superposed on the s/c trajectory in (c). We note in (a) the longer NKR activity at lower frequencies than at higher frequencies and the lack of emission during a large range of longitudes (NLS).

respect to the source direction [Ortega–Molina and Daigne, 1984; Leblanc and Daigne, 1985; Leblanc and Ladreiter, 1991]. Figure 1a shows a dynamic spectrum of the Neptunian emission during one rotation; black color indicates left–handed (LH) polarized emission, and white indicates right–handed (RH) activity. In this spectrum, there is an indication of two distinct sources, radiating independently and competing in intensity. The polarization pattern can also be seen in the fixed frequency plots (f=116.4 kHz, 174.0 kHz, and 250.8 kHz) in Figure 1b. The existence of two independently radiating sources is clearly shown around 0830 SCET (116.4 kHz) and around 1230 SCET (250.8 kHz), where the opposite polarized signals behave independently. We will therefore assume that there are two distinct sources.

Figure 1c shows the corresponding spacecraft magnetic latitude (δ_m) versus longitude (NLS) and versus magnetic longitude (λ_m) as well. The magnetic coordinates refer to the offset tilted dipole model (OTD2). Magnetic longitudes are counted eastward, and the 0° magnetic meridian is defined by the meridian linking the magnetic north pole to the rotational south pole of Neptune. The dipole ($M = 0.13$ G R_N^3) is tilted by about 45° with respect to the rotation axis and is offset by 0.5 Neptunian radii (R_N) [Ness et al., 1989].

Analyzing the observations in detail, we find that at DOY 236, 0700 SCET, a left–hand polarized emission came into view, especially around 150 kHz and 400 kHz, respectively. From Figure 1c we see that the spacecraft was at southern magnetic latitudes, which suggests that the LH radiation emanates from a southern hemisphere source in the extraordinary (R–X) mode (according to the orientation of the Neptunian magnetic dipole). At about 0900 SCET the left–handed signals are replaced by right–handed emission while the spacecraft crossed the magnetic equator to enter the northern magnetic hemisphere. There, we have mainly RH emission with a short episode of LH at 1200 SCET for frequencies around 400 kHz. The subsequent RH emission disappeared toward the lowest frequencies at 1500 SCET when the spacecraft reentered the southern hemisphere.

2.2 Observations around closest approach

Figure 2 shows the PRA observations on the day of encounter, DOY 237: Dynamic spectrum (panel a), fixed frequencies (panel b), and the corresponding spacecraft magnetic latitude (panel c). Just before closest approach (CA) the NKR emission vanished at all frequencies. After CA (0356 SCET) several different emissions have been identified. One component occurred at 0420 SCET when the spacecraft crossed the magnetic equator (Figure 2b). This emission extended up to 400 kHz and has been identified as electron cyclotron harmonic (ECH) waves [Gurnett et al., 1989; Kurth et al., 1990; Sawyer et al., 1990] and ion cyclotron harmonic (ICH) waves [Barbosa et al., 1990]. At 0520 SCET, emission occurred at the outbound Voyager ring plane (RP) crossing. The smooth NKR emission generally reappeared at 0600 SCET, depending on frequency.

Two distinct, polarized emissions can be seen in Figure 2a: the RH component (here the sense of polarization has been corrected by taking into account the antenna–source geometry) was first occulted at 0330 SCET. The LH component, which occurred only at the lower frequencies (up to about 200 kHz), disappeared later on. The RH emission

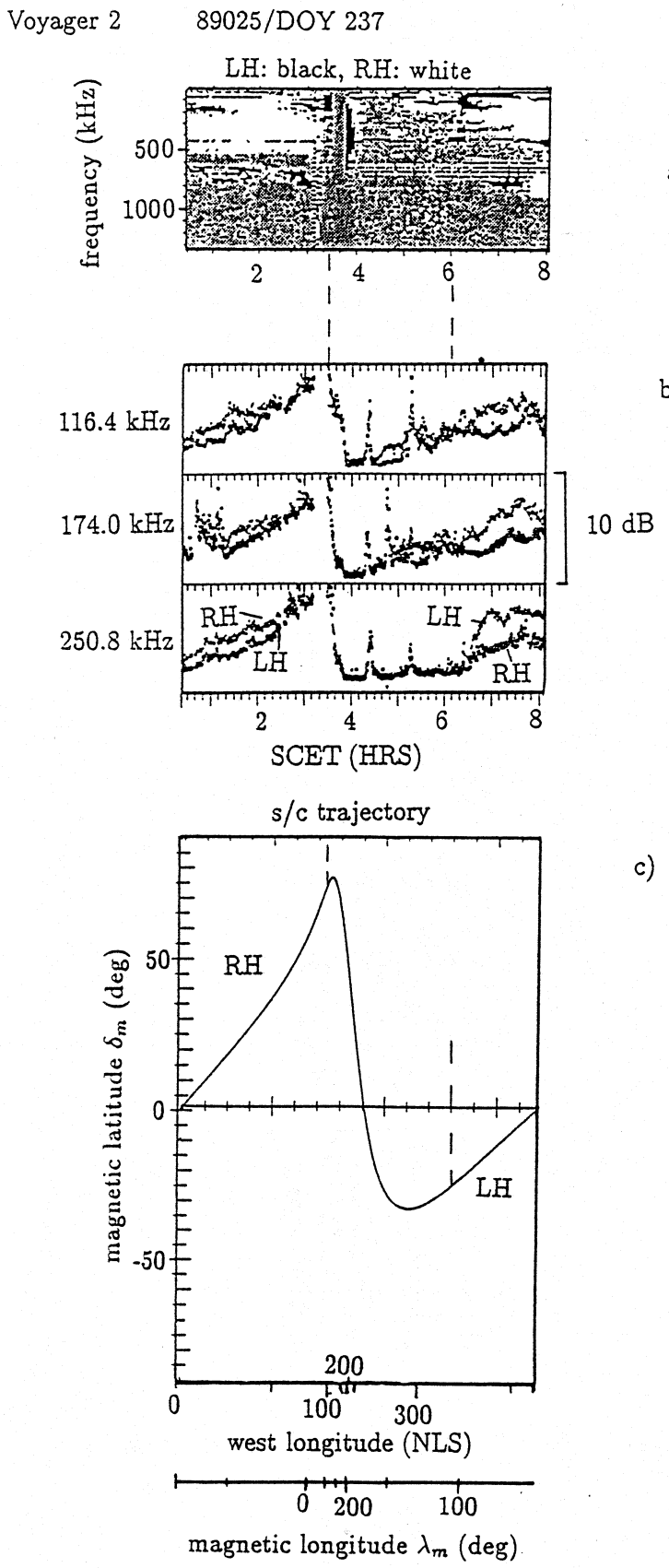

Figure 2: Same as Figure 1 but for the period around closest approach. We notice the sudden emission dropdown near 0330 SCET in (a) and (b) and the recurrence about 0600 SCET. The emission around 0400 SCET is interpreted as nonthermal continuum [Kurth et al., 1990].

vanished before the spacecraft entered magnetospheric regions where f_c exceeded the wave frequency. This cutoff is close to the R–X cutoff frequency since $f_c >> f_p$. In contrast the LH emission was not considerably affected by the $f = f_c$ crossing of the spacecraft. This is consistent with a RH emission propagating in the R–X mode and a LH emission propagating in the L–O mode.

3 Neptune's magnetic field

Shortly after the encounter of Voyager 2 with Neptune, it was recognized that a simple magnetic field model such as an offset tilted dipole (OTD2) model cannot account for the magnetic flux densities measured near closest approach, inside 1.2–3 R_N [Ness et al., 1989]. Multipole components considerably affect the magnetic field. Because of an unfavorable spacecraft trajectory (only the north polar regions were observed by V2 at small distances) one cannot accurately describe these magnetic multipoles with high–order terms in a spherical harmonic expansion. The current field model [OTD2 model, N.F. Ness, private communication, 1990] is based on magnetic field measurements from the magnetometer experiment [Behannon et al., 1977] within 3 to 15 R_N. The dipole moment is 0.13 G R_N^3, the dipole being tilted by about 45° with respect to the rotation axis and offset by 0.55 R_N. The result is a highly asymmetric field on the surface of Neptune. Because of the substantial offset of the magnetic dipole, B is more than 10 times higher in the southern pole than in the northern pole; a similar situation was observed for Uranus [Connerney et al., 1987]. Thus V2 explored regions of extremely low magnetic flux densities B during the encounter in the northern hemisphere. In addition, strong azimuthal field asymmetry occurs around the northern magnetic pole.

Because the OTD2 model was calculated with data obtained outside 3 R_N, it cannot be applied to regions close to the surface of the planet. However, the OTD2 model is sufficiently accurate for the description of the magnetic field near the lowest frequency source regions. This is especially true for sources at $f < 50$ kHz in the northern hemisphere, and for sources at $f < 200$ kHz in the southern hemisphere, since they are located at about 2 R_N from the planet center [Ladreiter et al., 1991]. For the location of the source regions we will therefore consider the frequency $f = 39.6$ kHz for the northern source and $f = 154.8$ kHz for the southern source.

4 Source location of smooth NKR

4.1 Method A: Location of the northern source from occultation observations near encounter

The exceptional conditions of the spacecraft–Neptune geometry during closest approach at 1.18 R_N have been used to locate the northern hemisphere sources solely by means of occultation of possible source candidates. Figure 3 illustrates how we define the radio horizon for a given spacecraft position. In order to be visible from the spacecraft, the

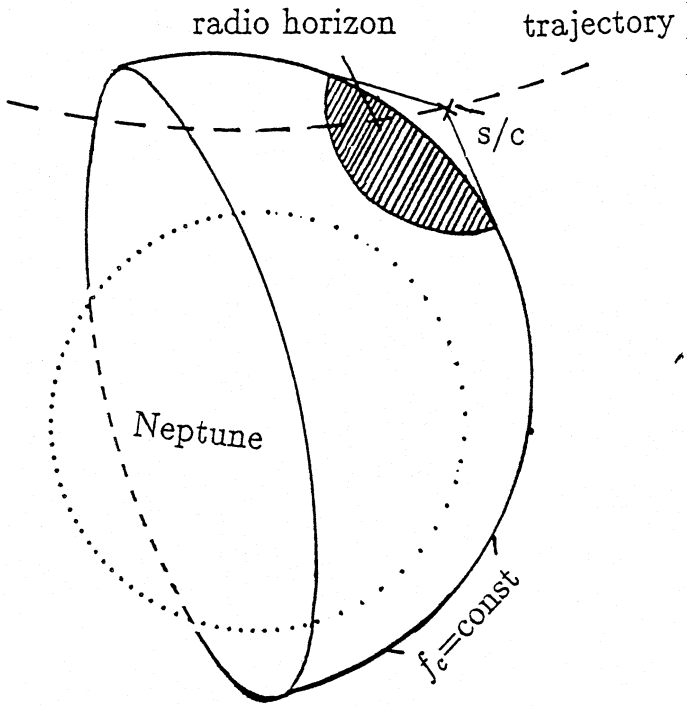

Figure 3: Illustration of the radio horizon calculation. The radio horizon is the region on the $f = f_c$–contour (f_c: cyclotron frequency as calculated from the OTD2 model, f: wave frequency) that is visible from the instantaneous spacecraft (s/c) position (hatched area).

radio source must be confined within the respective radio horizon (hatched area) which is defined by the OTD2 model and the corresponding gyrofrequency.

We have calculated the radio horizon as seen from Voyager 2 at two points along the V2 trajectory near CA for $f = 39.6$ kHz. The radio horizon on DOY 237, 0314 SCET, is shown in Figure 4a, the spacecraft–Neptune distance being 2.5 R_N. At that instant strong RH emission occurred (Figure 2a) before the emission dropdown at 0330 SCET, and thus the radio source started to go out of view of the spacecraft. However a great part of the source was still within the radio horizon (open area in Figure 4a). We note that only high magnetic latitude regions ($\delta_m > 40°$) in the northern magnetic hemisphere were in view by V2, implying that the source is at $\delta_m > 40°$. A similar conclusion was reached by Leblanc and Ladreiter [1991], who calculated the radio horizon for three spacecraft positions around the encounter for f=150 kHz. As the spacecraft continued to approach Neptune, the visible area of the $f_c = 39.6$ kHz level became smaller, and it shrunk to zero when the spacecraft crossed the $f_c = 39.6$ kHz level at 0325 SCET.

After encounter, significant RH emission was again observed at 0600 SCET (r=6.24 R_N) shortly after the outbound ring plane crossing of the spacecraft. Our model predicts the reappearance of emission at 0645 SCET (Figure 4b) where the area of visibility begins to overlap that of Figure 4a. Thus we are able to conclude that the northern source is located at a magnetic latitude higher than 40 degrees.

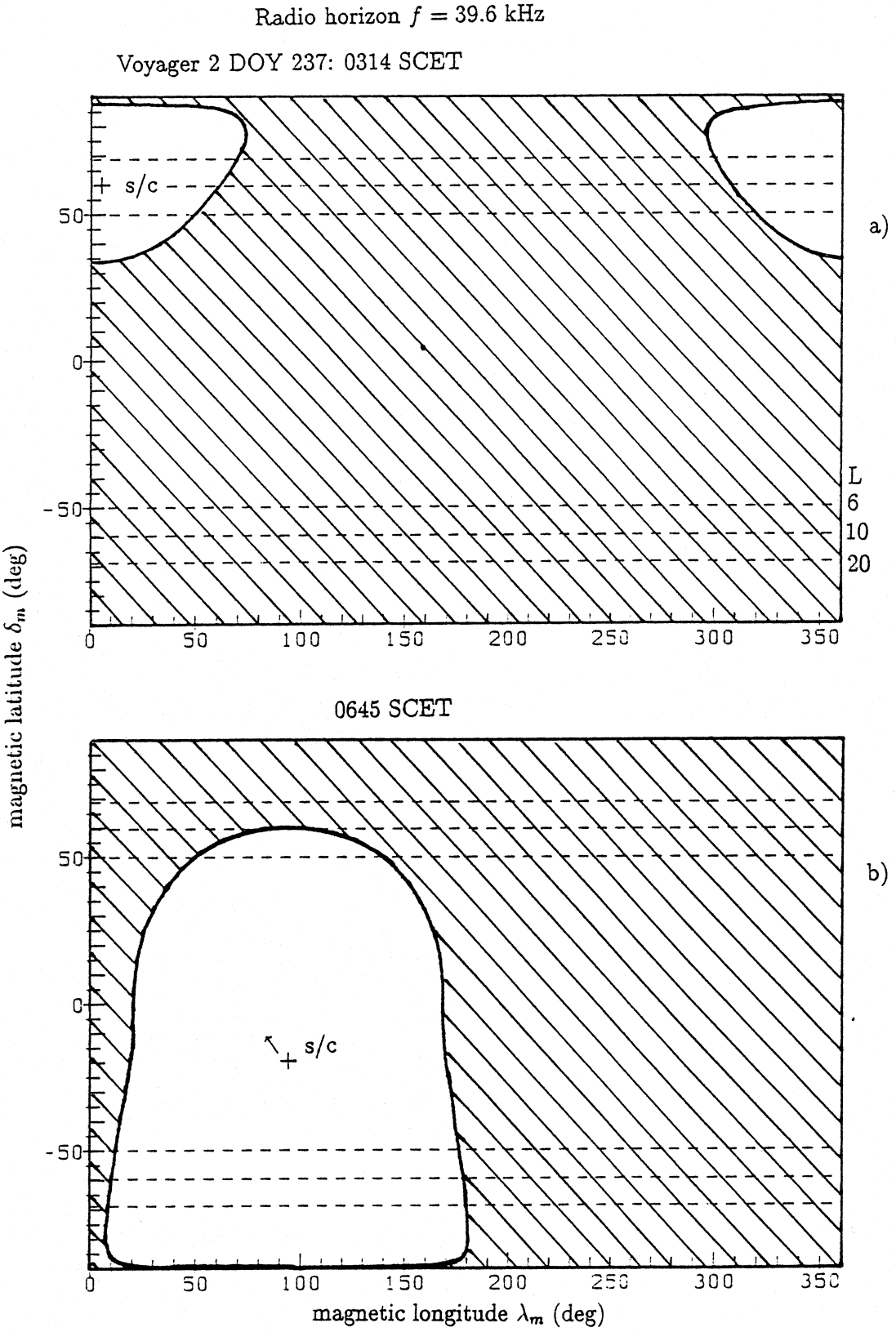

Figure 4: Radio horizons calculated for f=39.6 kHz (a) on DOY 237, 0314 SCET, when Voyager was at 2.5 R_N, and (b) on DOY 237, 0645 SCET, when Voyager was at 8.24 R_N. The arrow in (b) denotes the direction of the spacecraft trajectory.

4.2 Method B: Source location of the northern source by assuming a geometrical beaming model

We have assumed a geometrical beaming model as given in Gulkis and Carr, 1987 (Equation 2) to model the intensity profile near closest approach. We have assumed that the source is at a level where the ratio of the frequency to the gyrofrequency is 1.0 (the exact ratio is not critical to the results); the calculations were undertaken for f=39.6 kHz. The emission is assumed to be beamed within an emission cone with a large half–opening angle θ with respect to the magnetic field as shown in Figure 5. The observing spacecraft detected emission when the lobe of the emission cone crossed the observer. Two different lobe thicknesses $\Delta\theta$ (equal to half power width) have been considered. The sources are assumed to be distributed uniformly at all longitudes. For the calculation the continuous source distribution is replaced by 90 subsources. Refraction during propagation is not considered. The assumption of a hollow cone radiation model is justified by different studies of direct observations such as for Jupiter [Dulk, 1967], or of modeling the observed emissions of Jupiter [Menietti et al., 1984; Ladreiter and Leblanc, 1990], of Saturn [Galopeau et al., 1989], and of Uranus [Gulkis and Carr, 1987; Kaiser et al., 1987; Zarka and Lecacheux, 1987]. Such a beaming is predicted in the cyclotron maser mechanism [Wu and Lee, 1979; Wong et al., 1982], in particular for low–density magnetoplasma [Ladreiter, 1991], which accounts well for the radio observations of the different planets.

Figure 6 shows the modeled intensity profiles (dotted lines) for cone half angle $\theta = 70°$, two lobe thicknesses $\Delta\theta = 15°$ and 40°, and three source latitudes $L = 4$, $L = 6$, and $L = 10$, together with PRA observations (f = 39.6 kHz) around V2 closest approach. Since we are concerned here with the northern source, only the RH emission is considered, and represented by a thick line. At the beginning of DOY 237 the observed RH intensity

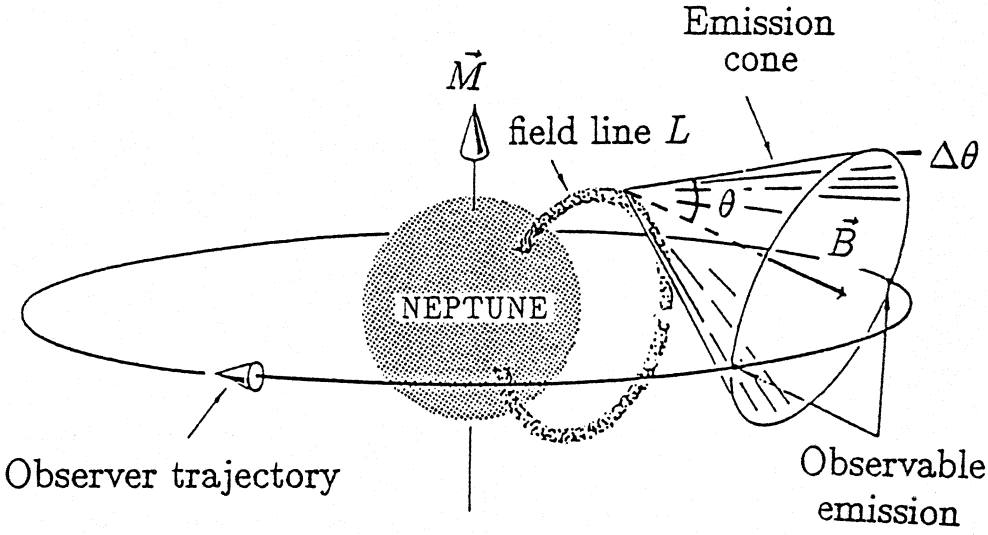

Figure 5: Sketch of emission beamed in a hollow cone pattern. Emission is observed when the spacecraft crosses the lobe of the emission cone characterized by the cone half angle θ and lobe thickness $\Delta\theta$. Assuming a lobe profile function according to Gulkis and Carr [1987] we can calculate the intensity profile.

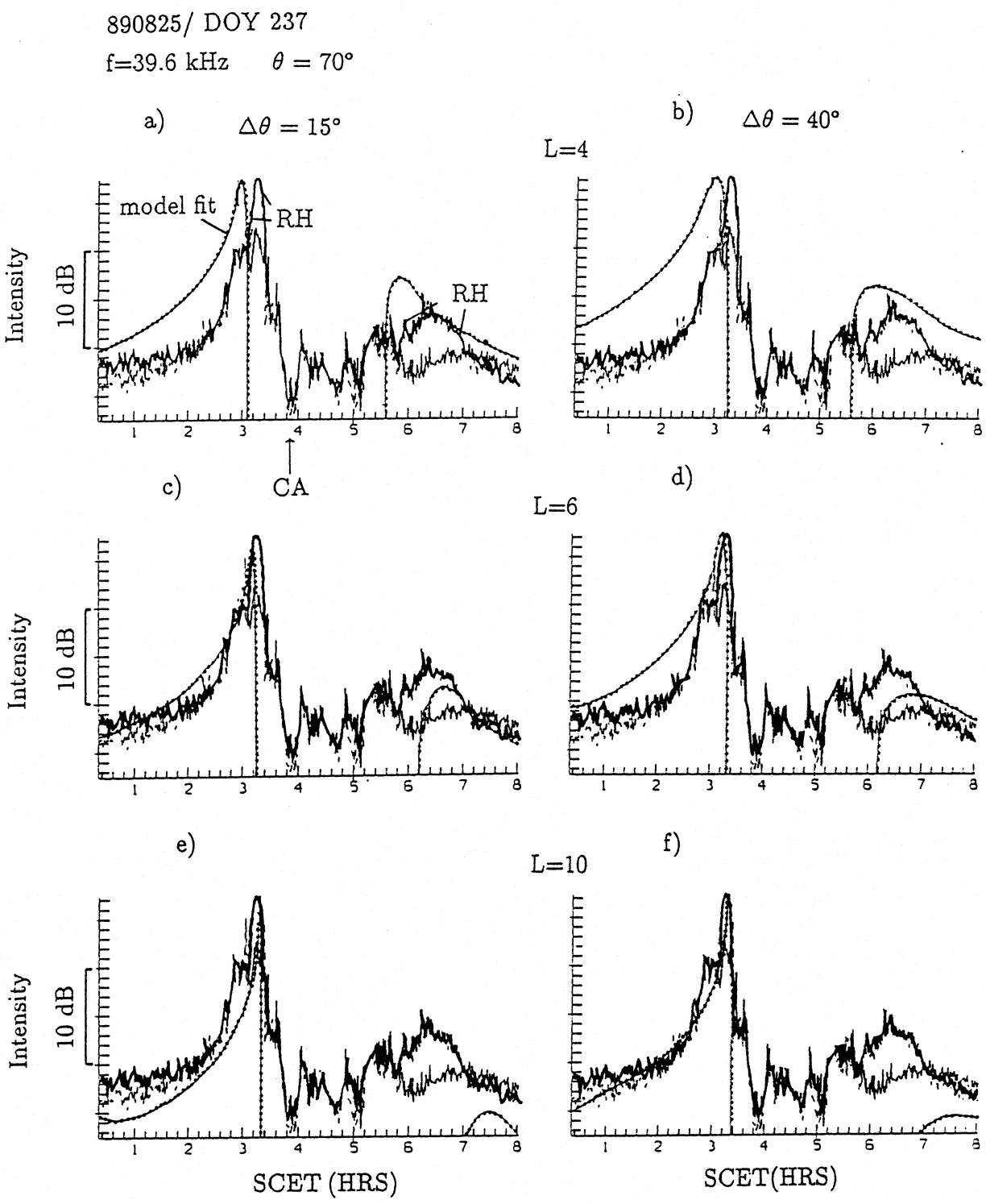

Figure 6: Comparison of PRA observations at $f = 39.6$ kHz near encounter (thick line for RH and thin line for LH emission) and model fits assuming a hollow cone emission (dotted line) for radio sources in the northern hemisphere. The selected parameters are a cone half angle $\theta = 70°$, with a lobe thickness $\Delta\theta = 15°$ and $40°$. Sources are distributed over all longitudes at L shells of 4, 6, and 10. Sources at L=6 (beam half width of 15°) best fit the RH observations. The data containing the ring plane crossing and electron cyclotron harmonic waves are deleted for clarity.

increased monotonically to a maximum just before the emission dropout at 0350 SCET. This increase in intensity is a consequence of the continuous approach to the radio sources and the beaming pattern of the emission. The emission occurring between 0325 and 0400 SCET was mainly LH polarized and has been interpreted as escaping continuum radiation [Kurth et al., 1990]. Between 0400 and 0600 SCET, mainly electrostatic noise occurred, including the ring plane crossing at about 0520 SCET. After 0600 SCET, right–hand polarized radio waves were again observed.

We note the consistency of the observations with the hollow cone beaming model, however, the observed features are better modeled only for selected parameters. The times of the RH emission dropout before CA and the reappearance after CA are most critical to the model fits. Thus these two events can be used to select the best L value for the source location and the best cone half thickness $\Delta\theta$. In particular, the modeled emission onset after CA is sensitive to the source location. For $L = 4$ it is predicted too early, for $L = 10$ it is predicted too late, but $L = 6$ gives a satisfactory fit. The beam thickness $\Delta\theta$ does not seem to be a very sensitive parameter; a somewhat better fit is obtained for $\Delta\theta = 15°$ than for $\Delta\theta = 40°$.

For the intensity modeling in Figure 6 we have assumed that the radio sources are distributed uniformly along all magnetic longitudes, the cone half–opening angle being always 70°. We additionaly have considered sources which are not active along the whole range of longitudes and studied the effect of varying θ. We have varied the parameters L, θ, $\Delta\theta$, and $\Delta\lambda_m$ (defining the longitudinal extent of the source) in a systematic way and found that the good fits (as shown in Figure 6) are generally maintained for $\theta \geq 50°$. Most importantly, we noted that the model fits are nearly unchanged when we allow the source to be active only from $-90° < \lambda_m < 90°$. We verified that the intensity profile modeled in Figure 6 is mainly the result of subsources confined within $-90°$ to $90°$ magnetic longitude.

The results derived from the radio horizon calculations (Method A), as well as the model fits from the geometrical beaming model (Method B), are consistent and imply a northern source location at $\delta_m > 40°$, possibly in the vicinity of magnetic field lines near L=6. More accurate results cannot be given because of the uncertainties of the OTD2 model. We have considered here only the RH observations near encounter; however, we verified in a previous work [Ladreiter et al., 1991] that the recurrent RH emission (Figure 1) can also be described with the above northern source location.

4.3 Method C: Determination of location of the southern source

To locate the sources in the southern hemisphere, we used Voyager's large excursions to high southern magnetic latitudes (see Figure 1c). During one Neptunian rotation there is a lack of emission from 160° to 320° NLS when the spacecraft was outside all emission beams. We have taken advantage of this lack of emission, when the spacecraft was predominantly in the southern hemisphere, to develop a method for locating the southern source.

For a given spacecraft position S_1 when no emission was detected, we have calculated the angle θ_1 between the local magnetic field direction at a given point P_1 (denoting a source

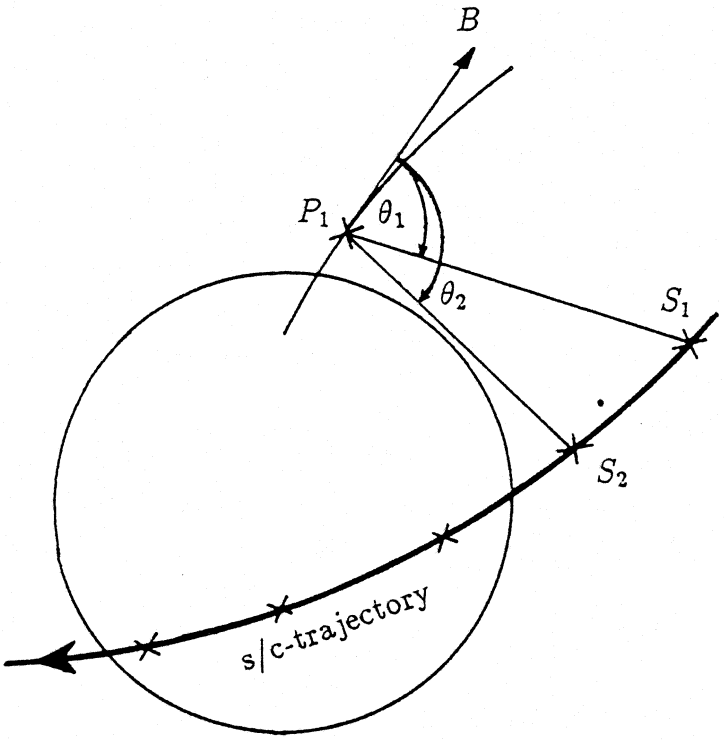

Figure 7: Geometry used for the determination of the southern sources. We derived the angles θ_1, $\theta_2, \ldots$ between the magnetic field direction at the point P_1 and the s/c positions S_1, S_2, ... We then calculated the range of angles $\theta_{\min}$, $\theta_{\max}$ where P_1 was viewed from Voyager during times of no emission activity.

candidate) and the actual spacecraft position S_1 as shown in Figure 7. We did those calculations for all spacecraft positions where no emission was observed (we simulated the continuous spacecraft trajectory from 160° to 320° NLS by 108 equidistant spacecraft positions S_1 to S_{108}). From the resulting angles (θ_1, $\theta_2 \ldots \theta_{108}$) we determined the angles $\theta_{\min}$ and $\theta_{\max}$ which define the range of angles (directions) where P_1 was viewed from V2 during the emission gap. If, for P_1, the range of angles [$\theta_{\min}$, $\theta_{\max}$] is from 0° to 90°, that means that P_1 was viewed from all directions between 0° and 90° during the period where no emission was observed. We can then definitely state that P_1 cannot be a source of radio emission since any radiation must leave P_1 within a wave normal angle between 0° and 90°. This method of eliminating possible sources is powerful, particularly if the spacecraft explores a large range of magnetic latitudes during times of no observable radio emission. This was the case during the V2 Uranus and Neptune flybys.

We have calculated $\theta_{\min}$ and $\theta_{\max}$ using the trajectory during the emission gap from almost 160° to 320° NLS. We have performed our analysis for the low–frequency emission in order to maintain the validity of the OTD2 model (section 3). We chose 154.8 kHz, where the LH emission emanating from the southern hemisphere was easily visible. Figure 8 shows $\theta_{\min}$ and $\theta_{\max}$ contours for the Neptunian southern hemisphere calculated from 108 points representing the spacecraft (s/c) trajectory (crosses). Let us now consider a realistic beaming of the emission where the wave normal angle at the source is in a direction somewhere between 50° and 85°. It is then possible to eliminate all the source candidates which were viewed from this angular range during times of no emission activity. This was the case for all sources which were viewed from $\theta_{\min} < 50°$ (as calculated in Figure 8a) and $\theta_{\max} > 85°$ (Figure 8b). The region in question is emphasized in Figure 8a (dotted area). Further, we can eliminate lower–latitude sources ($\delta_m > -40°$), since those sources

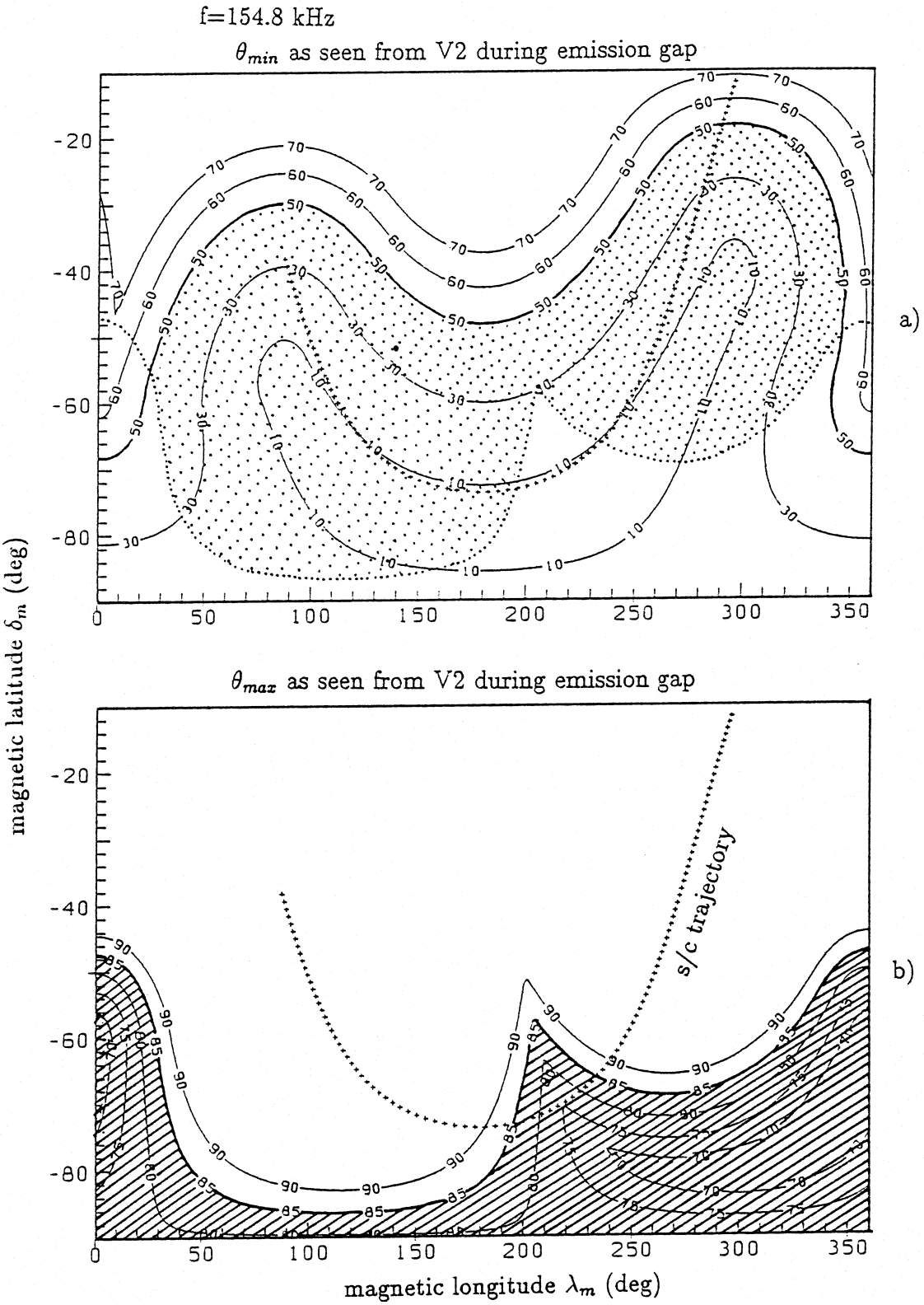

Figure 8: Calculation of the values (a) $\theta_{\min}$ and (b) $\theta_{\max}$ for $f = 154.8$ kHz during episodes of no NKR activity. The dotted area in (a) defines the region for which $\theta_{\min} < 50°$ and $\theta_{\max} > 85°$ (taken from (b)). Source locations in the hatched area in (b) are consistent with the observed emission gap and are compatible with a hollow cone model with large half–opening angles $50° < \theta < 85°$.

could not provide emission down to $f = 20$ kHz (calculated from the OTD2 model), as observed. Thus possible source candidates are restricted to high southern magnetic latitudes (hatched area in Figure 8b). From the knowledge of the other radio planets we may assume that it is unlikely that the sources are located very close to the magnetic south pole ($\delta_m < -85°$ corresponding to $L \gg 100$). Therefore we are left with a region limited in magnetic longitude from $\lambda_m = 200°$ to $\lambda_m = 40°$ and $\delta_m < -50°$, the possible extent of southern NKR source locations.

During this analysis we considered a hollow cone emission pattern with large half cone angles from $\theta = 50°$ to $85°$. The upper limit $\theta_{\max} = 85°$ instead of $\theta_{\max} = 90°$ is justified by noting that waves with $\theta > 85°$ are generally occulted by the $f = f_c$ contour and cannot therefore reach the observer. The plasma in the Neptunian magnetosphere has been found to be of low density [Belcher et al., 1989]. However, observations of whistlers in the Neptunian magnetosphere [Gurnett et al., 1989] imply a higher plasma density than already reported by Belcher et al. [1989]. In that case, as a consequence, the hollow cone angle could be narrowed by refraction, so that an upper limit with $\theta = 85°$ would still be appropriate.

5 Discussion

On the basis of the Voyager 2 PRA observations during the Neptune flyby at the end of August 1989, we derived important characteristics of the smooth kilometric radiation of Neptune. The emission pattern repeats with the Neptunian rotation period and is modulated by spacecraft emission beam crossings. The complex polarization pattern is consistent with two distinct radio sources, a northern and a southern one, which radiate independently in the extraordinary (R–X) mode and are competitive in intensity. No local time effect has been detected.

The main emphasis was laid on the source location of the emission. Thus three different methods were applied, taking advantage of the specific spacecraft–Neptune geometry near the Voyager encounter. To locate the radio sources we used the offset tilted dipole model (OTD2), but this model is valid only for $r > 3\ R_N$. The radio sources, however, are mainly located inside 3 R_N, closer to the Neptunian surface. To maintain the validity of the model we choose the low–frequency part of smooth NKR for our analysis.

Using the exceptionally close encounter of Voyager 2 (V2), we calculated the radio horizon for R–X waves ($f = 39.6$ kHz) for two selected spacecraft positions. This analysis implies the existence of a source at $\delta_m > 40°$ in the northern hemisphere. In addition we generated a geometrical beaming model where the sources are located at altitudes where the wave frequency is equal to the electron cyclotron frequency. We showed that the emission from the northern source can be described by a hollow cone beaming model, the half–opening angle being greater than $50°$. The best fits are obtained for sources at $L = 6$, but this result must be taken as provisional because of the error inherent in the OTD2 model. The longitudinal source extent is at least from $-90°$ to $90°$ magnetic longitude.

Taking advantage of the large emission gap observed during the spacecraft excursions into the southern magnetic hemisphere, we developed a method to locate the source of the LH

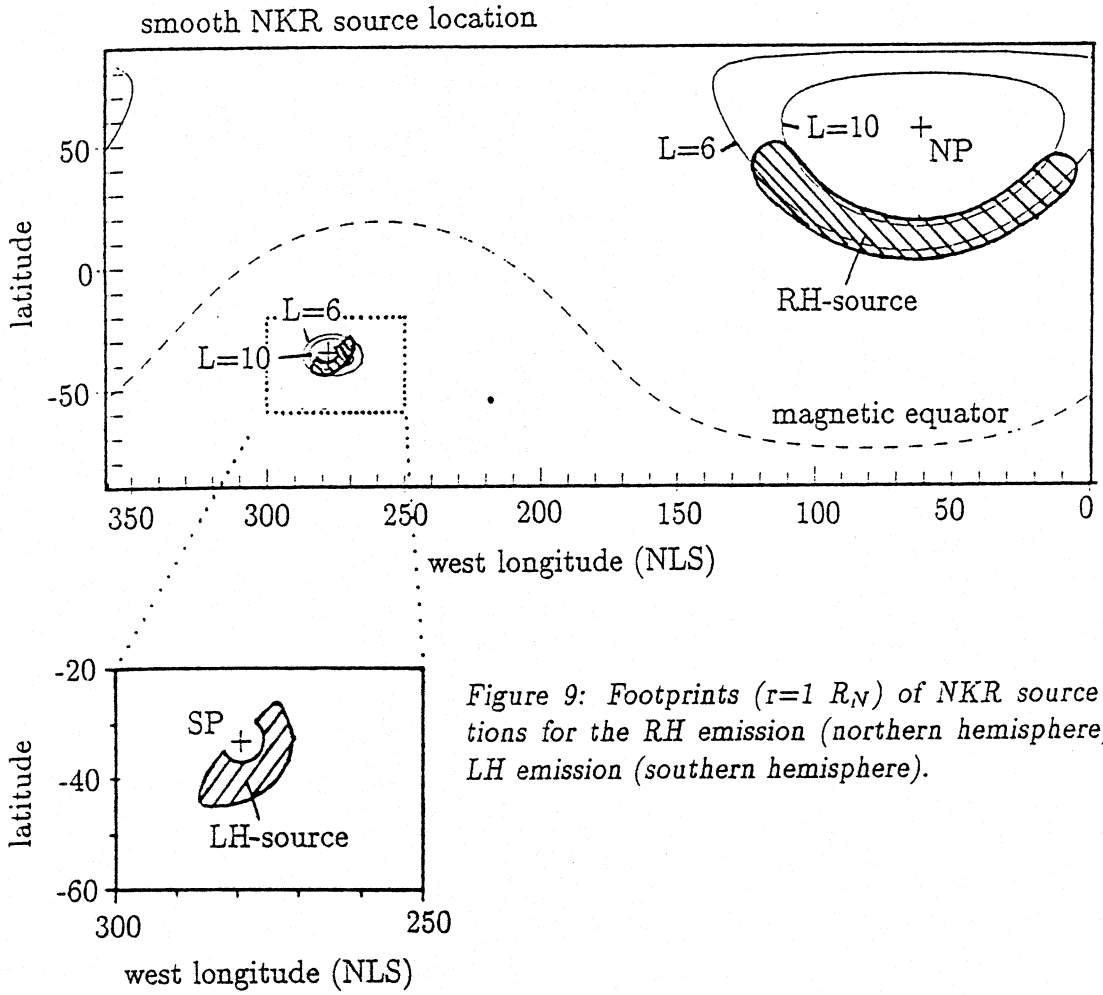

Figure 9: Footprints (r=1 R_N) of NKR source locations for the RH emission (northern hemisphere) and LH emission (southern hemisphere).

emission. We found that the source lies within a limited longitude range, possibly from 200° to 40° magnetic longitude at high magnetic latitudes ($\delta_m < -50°$). Northern and southern sources are therefore located at conjugate points, as has already been suggested by Sawyer et al. [1990]. The best fit is obtained for two different cone half–opening angles of the northern source (60°) and southern source (80°). This slight difference may reflect the different ratios f_p/f_c at both sources due to the asymmetric magnetic field configuration. The (theoretical) foot points (calculated with OTD–model at r=1 R_N) of the derived source locations are shown in Figure 9.

Planetary radio emissions are usually expected to emanate from the auroral zones within the magnetosphere. The Neptunian auroral zones have been identified by Broadfoot et al. [1989] using ultraviolet (UV) spectrometer observations of Neptune. Aurora were observed only on the dark side of Neptune at longitudes $\approx 30°$ and 200° NLS, and at high magnetic latitudes (L=14 to 16). We have not identified a local time dependence of the NKR emission nor observed any particular intensity enhancement around 30° and 200° NLS. This suggests that there is not a close relationship between the NKR sources and the UV aurora, and that their location might be different. This is consistent with our results which suggest that the radio sources must be located at lower magnetic latitudes,

along closed field lines (L=6 to 10).

In a previous work [Leblanc and Ladreiter, 1991] we also discussed the derived source locations in the framework of the emission's polarization, and it was found that the derived source locations and beaming properties account for two conjugate sources at L=6 to 10. Comparing our southern source locations to the sources of the bursty emission as derived by Farrell et al. [1990] we notice that they are partially overlapping. A similar situation exists at Uranus [Zarka and Lecacheux, 1987; Leblanc et al., 1987].

Acknowledgments: The authors thank N. F. Ness for providing the OTD2 model of Neptune's magnetic field. We are grateful to G. Dulk for helpful comments.

References

Barbosa, D. D., W. S. Kurth, I. H. Cairns, D. A. Gurnett, and R. L. Poynter, Electrostatic electron and ion cyclotron harmonic waves in Neptune's magnetosphere, *Geophys. Res. Lett.*, **17**, 1657, 1990.

Behannon, K. W., M. H. Acuña, L. F. Burlaga, R. P. Lepping, N. F. Ness, and F. M. Neubauer, Magnetic field measurements for Voyagers 1 and 2, *Space Sci. Rev.*, **21**, 235, 1977.

Belcher, J. W., et al., Plasma observations near Neptune: Initial results from Voyager 2, *Science*, **246**, 1478, 1989.

Broadfoot, A. L., S. K. Atreya, J. L. Bertaux, J. E. Blamont, A. J. Dessler, T. M. Donahue, W. T. Forrester, D. T. Hall, F. Herbert, J. B. Holberg, D. M. Hunten, V. A. Krasnopolsky, S. Linick, J. I. Lunine, J. C. McConnell, H. W. Moos, B. R. Sandel, N. M. Schneider, D. E. Shemansky, G. R. Smith, D. F. Strobel, R. V. Yelle, Ultraviolet spectrometer observations of Neptune and Triton, *Science*, **246**, 1459, 1989.

Connerney, J. E. P., M. H. Acuña, and N. F. Ness, The magnetic field of Uranus, *J. Geophys. Res.*, **92**, 15329, 1987.

Dulk, G. A., Apparent changes in the rotation rate of Jupiter, *Icarus*, **7**, 173, 1967.

Farrell, W. M., M. D. Desch, and M. L. Kaiser, Field–independent source localization of Neptune's radio bursts, *J. Geophys. Res.*, **95**, 19143, 1990.

Galopeau, P., P. Zarka, and D. Le Queau, Theoretical model of Saturn's kilometric radiation spectrum, *J. Geophys. Res.*, **94**, 8739, 1989.

Gulkis, S., and T. D. Carr, The main source of radio emission from the magnetosphere of Uranus, *J. Geophys. Res.*, **92**, 15159, 1987.

Gurnett, D. A., W. S. Kurth, R. L. Poynter, L. J. Granroth, I. H. Cairns, W. M. Macek, S. L. Moses, F. V. Coroniti, C. F. Kennel, and D. D. Barbosa, First plasma wave observations at Neptune, *Science*, **246,** 1494, 1989.

Kaiser, M. L., M. D. Desch, and S. A. Curtis, The sources of Uranus' dominant nightside radio emission, *J. Geophys. Res.*, **92,** 15169, 1987.

Kurth, W. S., D. D. Barbosa, D. A. Gurnett, R. L. Poynter, and I. H. Cairns, Low–frequency radio emissions at Neptune, *Geophys. Res. Lett.*, **17**, 1649, 1990.

Ladreiter, H. P., The cyclotron maser instability – Application to low–density magnetoplasmas, *Astrophys. J.*, **370,** 419, 1991.

Ladreiter, H. P., and Y. Leblanc, Modeling of the Jovian hectometric radiation: A three–dimensional study, *Ann. Geophys.*, **8**(7–8), 477, 1990.

Ladreiter, H. P., Y. Leblanc, G. K. F. Rabl, and H. O. Rucker, Emission characteristics and source location of the smooth Neptunian kilometric radiation, *J. Geophys. Res.*, **96**, 19101, 1991.

Leblanc, Y., M. G. Aubier, A. Ortega–Molina, and A. Lecacheux, Overview of the Uranian radio emissions: Polarization and constraints on source location, *J. Geophys. Res.*, **92**, 15125, 1987.

Leblanc, Y., and G. Daigne, Broadband Jovian kilometric radiation: New results on polarization and beaming, *J. Geophys. Res.*, **90**, 12073, 1985.

Leblanc, Y., and H. P. Ladreiter, Neptune's radio emissions, *Adv. Space Res.,* in press, 1991.

Menietti, J. D., J. L. Green, S. Gulkis, and N. F. Six, Jovian decametric arcs: An estimate of the required wave normal angles from three–dimensional ray–tracing, *J. Geophys. Res*, **89**, 9089, 1984.

Ness, N. F., M. H. Acuña, L. F. Burlaga, J. E. P. Connerney, R. P. Lepping, and F. M. Neubauer, The magnetic field of Neptune, *Science*, **246**, 1473, 1989.

Ortega–Molina, A., and G. Daigne, Polarization response od two crossed monopoles on a spacecraft, *Astron. Astrophys.*, **130**, 301, 1984.

Sawyer, C., J. W. Warwick, and J. H. Romig, Smooth radio emission and a new emission at Neptune, *Geophys. Res. Lett.*, **17**, 1645, 1990.

Warwick, J. W., J. B. Pearce, R. G. Peltzer, and A. C. Riddle, Planetary radio astronomy experiment for Voyager missions, *Space Sci. Rev.*, **21**, 309, 1977.

Warwick, J. W., et al., Voyager planetary radio astronomy at Neptune, *Science*, **246**, 1498, 1989.

Wong, H. K., C. S. Wu, F. J. Ke, R. S. Schneider, and L. F. Ziebell, Electromagnetic cyclotron–loss–cone instability associated with weakly relativistic electrons, *J. Plasma Phys.*, **28**, 503, 1982.

Wu, C. S., and L. C. Lee, A theory of the terrestrial kilometric radiation, *Astrophys. J.*, **230**, 621, 1979.

Zarka, P., and A. Lecacheux, Beaming of Uranian nightside kilometric radio emission and inferred source location, *J. Geophys. Res.*, **92**, 15177, 1987.